A New Approach of Using Porous Bleed Boundary Conditions - Application of Local Porosity

Julian Giehler, Pierre Grenson, Reynald Bur

A New Approach of Using Porous Bleed Boundary Conditions - Application of Local Porosity

Julian Giehler, Pierre Grenson, and Reynald Bur

DAAA, ONERA, Université Paris Saclay, 92190 Meudon, France
julian.giehler@onera.fr
pierre.grenson@onera.fr
reynald.bur@onera.fr

Abstract. Porous bleed systems are widely used to mitigate the shock-induced boundary layer separation, e.g., in supersonic air intakes. However, the complex geometry makes simulations expensive and motivates the application of suitable models. Existing models are based on applying a continuous blowing/suction boundary condition (continuous porosity) along the porous plate, leading to an overestimation of the boundary layer thinning. The new method using distributed suction by a local porosity is applied on a Mach 1.6 supersonic flow and improves the prediction of the effect on the boundary layer significantly. In contrast to the existing methods, the wall shear stress is not overestimated, and the boundary layer profiles downstream of the bleed region are better reproduced. Moreover, all expansion fans and barrier shocks caused by the bleed holes are captured.

Keywords: Porous bleed, Suction, Flow control, Boundary condition, Supersonic flow

1 Introduction

Porous bleed systems are a commonly used and proven technology to mitigate shock-induced boundary layer separations in supersonic air intakes. The general principle is the removal of low-momentum flow close to the wall by placing a porous plate below the shock foot to suck air through tiny holes in a lower-pressured cavity. However, estimating the so-called bleed mass flow rate and forecasting the impact on the boundary layer are challenging since simulations of the complete system are expensive in terms of computational costs. Typical systems consist of hundreds of holes with a diameter approximately the size of the (compressible) boundary layer displacement thickness. This results in a large number of cells required to model the geometry and makes even Reynolds-Averaged Navier-Stokes (RANS) simulations too cost- and time-consuming for a pre-design of an air intake.

As early as the first numerical simulations on porous bleed systems were performed, bleed models were proposed as the computational resources were insufficient to simulate the flow inside the holes [1–3]. These models are utilized as a sucking/blowing boundary condition generally dependent on the cavity plenum

pressure and the external wall pressure. In recent years, the modeling approaches improved due to more extensive computational resources and (numerical) studies investigating the flow behavior through the porous plate [4–6]. Nevertheless, existing models still lack reproducing the flow field obtained in reality. Geometrical parameters or inflow conditions (boundary layer properties) are often not considered in the computation of the bleed mass flow rate.
Moreover, the effect on the boundary layer needs to be taken into account, which can result in a bad design of the bleed system. Consequently, a new modeling approach is needed to mimic the complex flow physics correctly. In the current study, we propose a new approach to implement bleed boundary conditions using a more realistic local distribution of suction.
This paper is divided into six sections. Section 2 introduces the investigated physical problem. Sec. 3 gives a brief overview of the drawbacks of using a continuous porosity for all cells. The new methodology of the local porosity is described in Sec. 4 before showing the results of the new approach in Sec. 5. Our conclusions and outlooks to future work are drawn in the final section.

2 Investigated physical problem

The investigated problem is a turbulent supersonic flow on a flat plate with a porous bleed region. In this scenario, the porous bleed aims to thin the boundary layer, similar to the application on a supersonic air intake upstream of a shock. Fig. 1 illustrates the investigated domain. A turbulent boundary layer profile with a Mach number of $M = 1.6$, generated in a previous flat plate simulation, is applied as an inflow condition. The porous plate has a length of $L_p = 40\,\mathrm{mm}$, and is located with an offset of 40 mm to the inlet. In the span, the domain size corresponds to the distance between two lines of holes. On the center planes of the holes, symmetry is assumed.
The boundary layer properties (boundary layer thickness δ_{99}, displacement thickness δ_1, momentum thickness δ_2, and shape factor $H = \delta_1/\delta_2$) are extracted 5 mm upstream of the first hole and shown in Tab. 1. Moreover, the total pressure p_t and the total Temperature T_t are given.

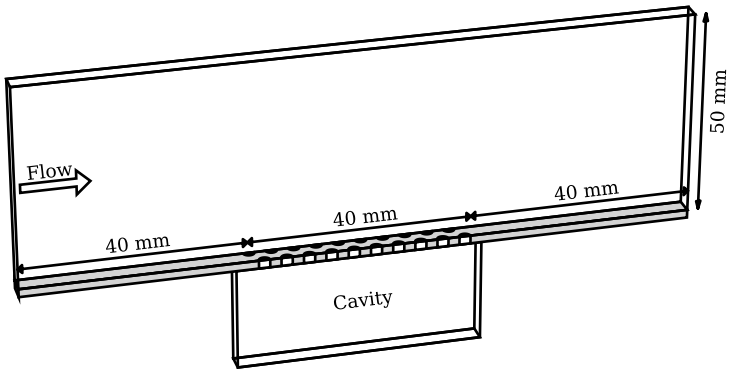

Fig. 1: Schematic of investigated numerical domain

M	p_t	T_t	Re_{δ_2}	δ_{99}	δ_1	δ_2	H
1.6	93 000 Pa	300 K	5450	4.20 mm	0.57 mm	0.42 mm	1.36

Table 1: Flow properties 5 mm upstream of the first bleed hole

In most applications, the bleed mass flow rate is determined by fixing a plenum exit area that is choked. As a result, the static pressure inside the cavity plenum changes until a mass balance between the mass flow rate entering the cavity through the porous plate and the mass exiting through the nozzle sets in. For the simulations, a throat ratio TR is defined, which corresponds to the ratio

$$TR = \frac{A_{pl,ex}}{A_{bl}} \tag{1}$$

of the plenum exit area $A_{pl,ex}$ and the bleed area A_{bl}, which is the sum of all hole areas.

3 Drawbacks of continuous porosity boundary conditions

In our previous study [7], several bleed models were implemented within the compressible multi-block structured Safran-ONERA finite-volume solver **elsA**. The turbulence is modeled using the Spalart-Allmaras turbulence model with constitutive relation [8]. In Fig. 2, the implemented boundary condition using the model of Slater [4] (Fig. 2c) is compared to two reference simulations with

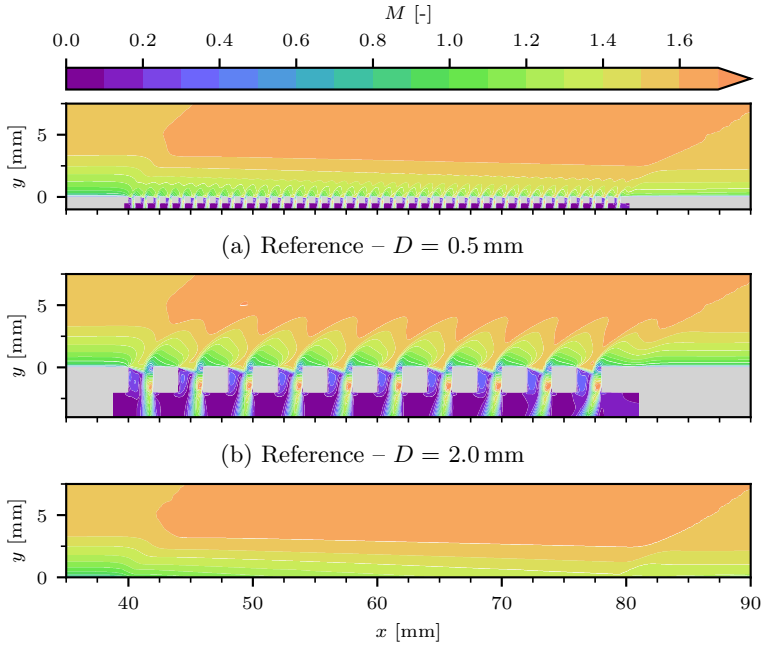

(a) Reference – $D = 0.5$ mm

(b) Reference – $D = 2.0$ mm

(c) Boundary condition – Slater [4]

Fig. 2: Mach contour fields for two reference simulations and applied boundary condition

hole diameters $D = 0.5\,\mathrm{mm}$ (Fig. 2a) and $D = 2.0\,\mathrm{mm}$ (Fig. 2b) for a throat ratio $TR = 0.7$. In the reference simulations, the hole contour is taken into account, and the holes are included in the mesh (see Giehler et al. [9]). In contrast, the boundary conditions are applied on a solid wall using source terms in the first layer of cells. All simulations are performed under steady-state conditions.

At first glance, all simulations show the same flow topology: a thinning of the boundary layer provoking an expansion fan at the beginning and a trailing shock wave at the end of the bleed region. While only one expansion fan and trailing shock are apparent in the simulation with the boundary condition, multiple shock waves and expansions caused by the holes are visible in the reference simulations. The larger the holes, the more pronounced these phenomena. A closer look at the flow downstream of the plate reveals a higher momentum in the vicinity of the wall compared to the reference simulations. Also, the diameter strongly influences the shape of the boundary layer, respectively the momentum close to the wall, as shown in our previous paper [9]. However, the model of Slater [4] does not consider any geometrical parameter other than the porosity level, which is the wall area fraction covered by the bleed holes. Thus, the flow field is assumed to be equal regardless the hole diameter or hole pattern.

The differences between boundary conditions and reference simulations are shown in more detail in Fig. 3 for several bleed models [4–6, 10–12]. The wall shear stress τ_w along the length of the porous plate L_p is detailed in Fig. 3a. A significant overestimation of the wall shear stress by using the boundary condition with the different bleed models is notable, caused by the uniform suction along the plate. Contrary to reality, the suction is not locally distributed but uniformly applied, and its mass flux is corrected using the porosity level of the plate. The higher the estimated mass flux of the models (see Tab. 2), the higher the obtained wall shear stress in the simulations. Moreover, the trailing shock is stronger for higher bleed mass fluxes resulting in a more significant drop of the wall shear stress at the end of the plate.

A look at the boundary layer profiles in Fig. 3b reveals a substantial deviation from the reference simulations for the boundary conditions. Independently of

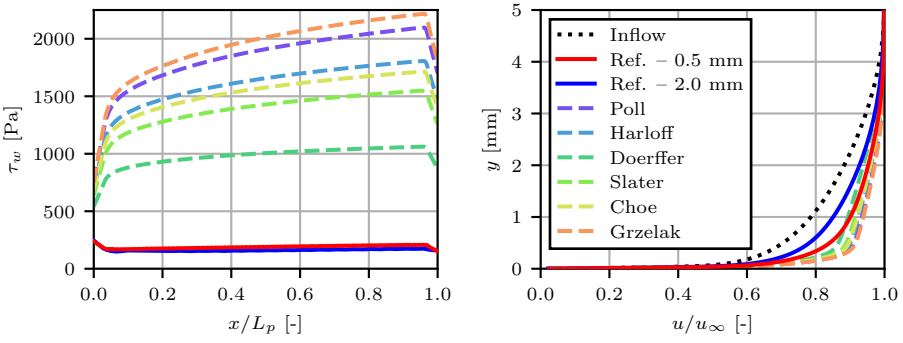

(a) Wall shear stress

(b) Boundary layer 10 mm downstream

Fig. 3: Comparison of continuous porosity boundary conditions with reference simulations

	Reference		**Boundary condition**					
	0.5 mm	2.0 mm	Poll	Harloff	Doerffer	Slater	Choe	Grzelak
H [-]	1.27	1.30	1.25	1.24	1.23	1.24	1.24	1.25
q_{bl} [kg/m^{2}s]	19.8	19.3	24.4	21.2	13.0	18.3	20.1	25.8
p_{pl} [Pa]	12 110	12 060	14 880	12 890	7930	11 120	12 260	15 680

Table 2: Boundary layer shape factor H extracted 10 mm downstream of the bleed region, bleed mass flux q_{bl}, and plenum pressure p_{pl}

the used model, the boundary layer profiles downstream of the bleed region are significantly fuller. As indicated in [7], the flow momentum close to the wall is overestimated. Moreover, we see a strong variation caused by the hole diameter, which is not captured by the continuous porosity boundary conditions.
Tab. 2 evidences the overperformance of the continuous porosity boundary condition. The shape factor is underestimated for all boundary conditions compared to the reference simulations, which indicates a more effective control than in reality. This effect is independent of the bleed mass flux. No matter if the bleed mass flux is over- or underestimated, applying the continuous porosity boundary condition leads to fuller profiles downstream of the bleed region. The prediction of the plenum pressure is in line with the prediction of the bleed mass flux. An overestimation of the mass flux leads to overestimating the plenum pressure.
The underestimation of the shape factor is a severe problem for pre-designing a supersonic air intake, where the porous bleed is applied to mitigate the shock-induced flow separation. The estimated overperformance of the system may lead to an undersized system, which could be unable to achieve the desired control effect.

4 Methodology for the local porosity

The principle of the local porosity is the discrete modeling of the hole contour with a pre-defined number of cells as schematically illustrated in Fig. 4. All cells with the cell center inside the hole contour are categorized as hole cells which means that suction is applied. All other patch cells are viscous walls. This procedure aims to enable the discrete modeling of the bleed holes on a simple, structured mesh.
For the current study, one hole is modeled by 10 cells streamwise and 6 cells in the spanwise direction. The higher streamwise resolution aims to accurately capture the flow phenomena as the expansion fan at the hole opening and the

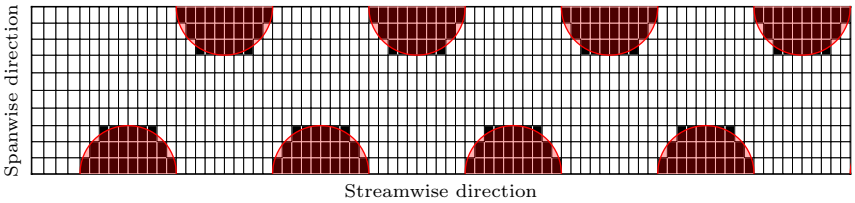

Fig. 4: Schematic of local porosity: black cells correspond to suction cells, white cells to solid wall; red circle illustrates theoretical hole position

Hole diameter	Reference	Local porosity	Continuous porosity
0.5 mm	5.1 M.	0.8 M.	<0.1 M.
2.0 mm	2.4 M.	0.3 M.	

Table 3: Comparison of the mesh sizes for the different methods

barrier shock at the rear edge of the hole. In the spanwise direction, a lower impact of the mesh resolution is assumed. Moreover, a low number of cells is preferred to increase the savings in computational costs compared to the reference simulations. The total mesh size depends on the hole diameter and increases for smaller holes (similar to the three-dimensional reference simulations). Tab. 3 shows the number of cells for the different configurations. The savings using the local porosity are approximately one order of magnitude compared to the reference simulations. However, the new method requires approximately one order of magnitude more cells than the simulations with continuous porosity, which are only two-dimensional.
The structured mesh is automatically generated by the in-house mesh-generator **Cassiopee**. Similarly to our previous work [7], the following source terms are added to the compressible Navier-Stokes equations to apply suction in the first row of cells. For the computation of the source terms, the cell size is taken into account by using the cell patch area A_c and the cell volume V_c.

$$\begin{aligned} &\text{Continuity:} && \frac{q_{bl} A_c}{V_c} \\ &\text{Momentum:} && \frac{q_{bl}^2 A_c}{\rho V_c} \\ &\text{Energy:} && \frac{q_{bl} c_p T_t A_c}{V_c} \end{aligned}$$

The bleed mass flux q_{bl} is computed in an external python script executed by the flow solver every 10th iteration. The bleed model applied for the local porosity boundary condition is the model of Choe et al. [5] since it has the best agreement with the reference simulations regarding the bleed mass flux and the plenum pressure. The required physical quantities for the model (static wall pressure and temperature) are extracted at the patch interface using the implemented extractors in **elsA**. The plenum pressure is found by fixing the (choked) plenum exit area and iteratively adjusting the plenum pressure until the mass balance is achieved.

5 Results and discussion

Both reference cases from Sec. 3 are simulated using the local porosity boundary condition. Fig. 5 shows the flow fields for the simulations, including the holes and the local porosity. The Mach number contours for a hole diameter of $D = 0.5\,\text{mm}$ are compared in Fig. 5a and 5b. The application of the local porosity shows a good fit with the reference simulation. The impact of the local suction is apparent in the vicinity of the wall, where the expansion fans and barrier shocks

generated by the holes are well reproduced. Compared to the continuous porosity (see Fig. 2c), the near-wall flow momentum is lower at the end of the bleed region, indicating a less full boundary layer profile.
More noticeable is the impact of the local porosity for a diameter of $D = 2\,\mathrm{mm}$ in Fig. 5d. For larger hole diameters, the expansion fans and shock penetrate the whole boundary layer and affect the flow field even outside the boundary layer. While the continuous porosity boundary condition cannot mirror this effect, applying the local porosity makes it visible. Similar to the reference simulation (Fig. 5c), only a slight boundary layer thinning is notable. Both expansion fans and barrier shocks are well reproduced, and the flow field fits very well.
However, a closer look at the wall reveals slight differences. For the application of

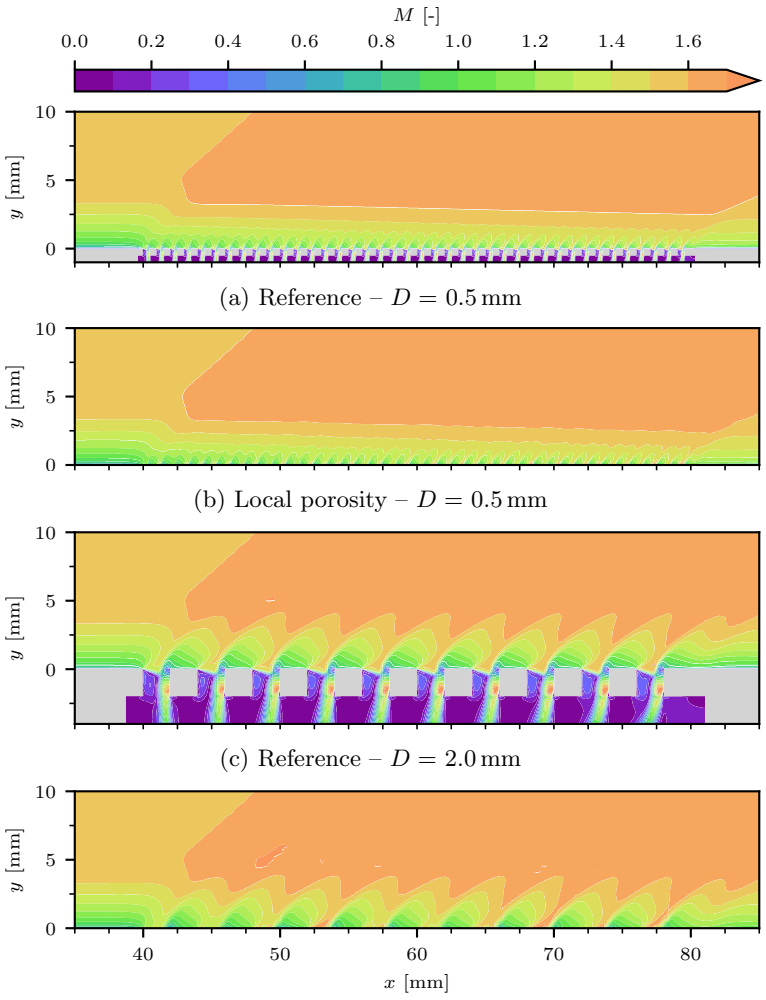

(a) Reference – $D = 0.5\,\mathrm{mm}$

(b) Local porosity – $D = 0.5\,\mathrm{mm}$

(c) Reference – $D = 2.0\,\mathrm{mm}$

(d) Local porosity – $D = 2.0\,\mathrm{mm}$

Fig. 5: Mach number contour fields for reference and local porosity

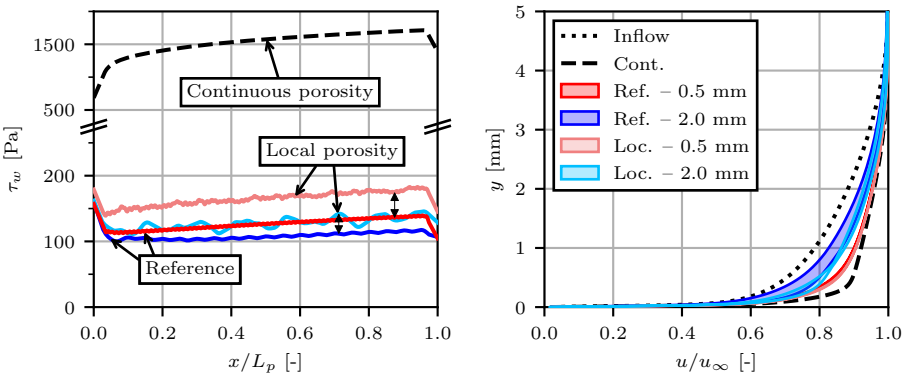

(a) Wall shear stress

(b) Boundary layer 10 mm downstream

Fig. 6: Comparison of the local porosity boundary condition with the reference simulations

the local porosity, higher Mach numbers are found at some holes in the vicinity of the wall. This is caused by an interaction of the source term, which generates a strong wall-normal flow momentum, and the wall boundary condition below that prevents outflow and, thus, a wall-normal flow component. For future investigations, the application of outflow/inflow boundary conditions is planned to eliminate such undesired (numerical) effects.

Further comparison of the local porosity boundary condition and the reference simulations are shown in Fig. 6. In contrast to the continuous porosity boundary condition, the prediction of the wall shear stress is close to the reference simulations by applying the local porosity (Fig. 6a). However, its amount is slightly overestimated. Already at the beginning of the plate, the wall shear stress is higher than in the reference simulations. Along the plate, the positive gradient of the wall shear stress is approximately the same. A reason for this behavior could be the low resolution in the spanwise direction. Further tests with higher resolutions in both stream- and spanwise directions are required to investigate the mesh influence. However, a higher resolution corresponds to higher computational costs. Thus, a compromise between accuracy and practicability needs to be made.

A view on Fig. 6b reveals a better fit of the boundary layer downstream of the bleed region than for the continuous porosity. The profile is only slightly fuller than in the reference simulation for the smaller hole diameter of $D = 0.5\,\mathrm{mm}$. Also, for $D = 2\,\mathrm{mm}$, the boundary layer profile computed using the local porosity is closer to the reference simulation but still fuller. Moreover, the variation of the boundary layer in the spanwise direction can be compared. Since the holes are locally distributed, three-dimensional effects are induced. These effects result in a profile variation along the span and can be modeled by the local porosity. Therefore, the range of all profiles is visualized. Compared to the reference simulations, the variation of the boundary layer profiles in the spanwise direction is lower for the local porosity. Again, the low spanwise resolution can be the reason and needs to be investigated.

	Reference		**Local porosity**		**Continuous**
	0.5 mm	2.0 mm	0.5 mm	2.0 mm	**porosity**
H [-]	1.27	1.30	1.26	1.28	1.24
q_{bl} [kg/m^{2}s]	19.8	19.3	20.6	21.1	20.1
			(+4.4 %)	(+9.3 %)	(+1.5 % / +4.2 %)
p_{pl} [Pa]	12 110	12 060	12 300	12 120	12 260
			(+1.6 %)	(+0.5 %)	(+1.2 % / +1.7 %)

Table 4: Boundary layer shape factor H extracted 10 mm downstream of the bleed region, bleed mass flux q_{bl}, and plenum pressure p_{pl}; relative errors are given in percentage of the reference simulations

The difference between the boundary layer profiles is also found in the shape factor, shown for the local porosity and the reference simulations in Tab. 4. For both hole diameters, the shape factor found downstream of the bleed region is slightly smaller than in the reference simulations. However, the predicted profiles are significantly closer to the reference than the continuous porosity.
Moreover, the predicted mass flux of the model of Choe et al. [5] is slightly higher by using the local porosity. Interestingly, the predicted mass flux is higher for large hole diameters, in contrast to the reference simulations and previous findings [9]. The larger the hole diameter, the stronger the barrier shock and, thus, the higher the static wall pressure downstream of the hole. Consequently, the model predicts a higher mass flux since the pressure difference from the external wall to the plenum is larger. The prediction of the static plenum pressure is only slightly different from the continuous porosity boundary condition and shows a good agreement.

6 Conclusion and future work

In this paper, a new approach to applying bleed boundary conditions has been implemented in the flow solver **elsA**, tested, and compared to reference simulations. The suction through the holes is locally applied by discretely modeling the hole contour and utilizing suction only on these pre-defined cells. In contrast to standard methods using continuous porosity on the patch, all expansion fans and barrier shocks induced by the holes are mirrored.
Using the local porosity boundary condition enables a more accurate prediction of the boundary layer profiles downstream of the bleed region. While the profiles are significantly fuller for the continuous porosity boundary condition, the present method only slightly overestimates the boundary layer thinning. Moreover, the wall shear stress along the porous plate is in the range of the reference simulations and not strongly overestimated like for the continuous boundary condition.
Future work is required to investigate the influence of the resolution of the holes. Therefore, a compromise between the saving of cells and accuracy needs to be found. Furthermore, the replacement of the source term and the viscous wall by local inflow and outflow boundary conditions is planned to eliminate numerical issues in the vicinity of the wall. Besides, the application of the new approach

will be tested to control of a shock-boundary layer interaction to examine the accuracy improvement in this complex flow pattern.

Acknowledgments

This project has received funding from the European Union's Horizon 2020 research and innovation programme under grant agreement No EC grant 860909.

Bibliography

[1] K. Abrahamson and D. Brower, "An empirical boundary condition for numerical simulation of porous plate bleed flows," in *26th Aerosp. Sci. Meet.* Reston, Virigina: American Institute of Aeronautics and Astronautics, jan 1988.

[2] W. J. Chyu, G. W. Howe, and T. I.-P. Shih, "Bleed-boundary conditions for numerically simulated mixed-compression supersonic inlet flow," *J. Propuls. Power*, vol. 8, no. 4, pp. 862–868, jul 1992.

[3] G. C. Paynter, D. A. Treiber, and W. D. Kneeling, "Modeling supersonic inlet boundary-layer bleed roughness," *J. Propuls. Power*, vol. 9, no. 4, pp. 622–627, jul 1993.

[4] J. W. Slater, "Improvements in Modeling 90-degree Bleed Holes for Supersonic Inlets," *J. Propuls. Power*, vol. 28, no. 4, pp. 773–781, jul 2012.

[5] Y. Choe, C. Kim, and K. Kim, "Effects of Optimized Bleed System on Supersonic Inlet Performance and Buzz," *J. Propuls. Power*, vol. 36, no. 2, pp. 211–222, mar 2020.

[6] J. Grzelak, P. P. Doerffer, and T. Lewandowski, "The efficiency of transpiration flow through perforated plate," *Aerosp. Sci. Technol.*, vol. 110, mar 2021.

[7] J. Giehler, P. Grenson, and R. Bur, "Porous Bleed Boundary Conditions for Shock-Induced Boundary Layer Separation Control," in *56th 3AF Int. Conf. Appl. Aerodyn.* Paris: Association Aéronautique et Astronautique de France, 2022.

[8] P. Spalart, "Strategies for turbulence modelling and simulations," *Int. J. Heat Fluid Flow*, vol. 21, no. 3, pp. 252–263, jun 2000.

[9] J. Giehler, P. Grenson, and R. Bur, "Parameter Influence on the Porous Bleed Performance with & without Shock-Boundary Layer Interaction," in *AIAA Aviat. 2022 Forum.* Reston, Virginia: American Institute of Aeronautics and Astronautics, 2022.

[10] D. I. A. Poll, M. Danks, and B. E. Humphreys, "Aerodynamic Performance of Laser Drilled Sheets," Univ. of Manchester. Aeronautical Engineering Group., Tech. Rep., 1992.

[11] G. J. Harloff and G. E. Smith, "Supersonic-inlet boundary-layer bleed flow," *AIAA J.*, vol. 34, no. 4, pp. 778–785, apr 1996.

[12] P. P. Doerffer and R. Bohning, "Modelling of perforated plate aerodynamics performance," *Aerosp. Sci. Technol.*, vol. 4, no. 8, pp. 525–534, nov 2000.